Jan ŠLAMBERGER[1], Mario VRAŽIĆ[2], Peter VIRTIČ[1],

University of Maribor, Faculty of Energy Technology (1), University of Zagreb, Faculty of Electrical Engineering and Computing (2)

Comparison of single- and double-layer windings in an axial flux permanent-magnet synchronous machine

***Abstract**. This paper deals with the comparison between single-layer and double-layer concentrated windings in an axial flux permanent magnet synchronous machine. The results are obtained using finite element method and present the differences in back electromotive force, cogging torque, detent force and static torque for both winding topologies.*

***Streszczenie.** W artykule przedstawiono porównanie między pojedyńczo- i podwójnie-warstwowymi uzwojeniami koncentrycznymi maszynach synchronicznych z magnesami trwałymi i strumieniem osiowym. Do tego porównania wykorzystano metodę elementów skończonych, a wyniki analizy prezentują różnice we wstecznej sile elektromotorycznej, momentach pulsacyjnych, sile zaczepu i momencie statycznym dla obu topologii uzwojenia. (**Porównanie pojedynczo- i podwójnie-warstwowych uzwojeń w maszynie synchronicznej z magnesami trwałymi i strumieniem osiowym**)*

Keywords: axial flux, permanent magnet, synchronous machine, winding.
Słowa kluczowe: strumień osiowy, magnes trwały, maszyna synchroniczna, uzwojenie.

doi:10.12915/pe.2014.12.41

Introduction

The concentrated windings in an axial flux permanent magnet synchronous machine (AFPMSM) may be wounded as single- or double-layer windings. In case of a single-layer winding only every second tooth is wounded, meanwhile in case of a double-layer winding every tooth is wounded (Fig. 1) [1]. The comparison of characteristics of AFPMSMs with single-layer and double-layer concentrated windings will be a focus of this paper. The proposed calculation method is based on finite element method (FEM), which can be used for diagnostics of the damage rotor elements of induction motor [2-3], inter-coil short circuit detection [4], unsymmetrical load calculation [5], and in automated detection of the anomalies [6-7]. AFPMSM can be used also for the wind energy exploitation in Slovenia [8-9].

The AFPMSMs used in this paper have the same shape and amount of cooper and rotor iron cores. The cogging torque, the back electromotive force, the detent force and the static torque are calculated with FEM using software package ANSYS workbench V14.0. The procedure of numerical calculations was verified with analytical methods and measurements in [10] and [11].

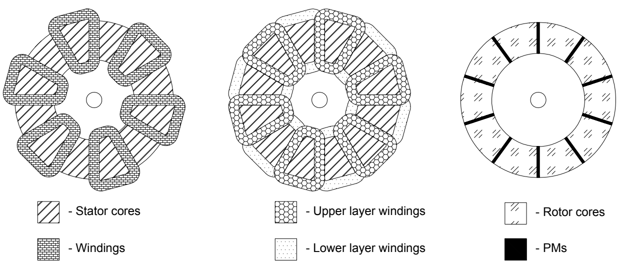

Fig.1. Topologies of AFPMSMs

Maxwell's equation for magnetic field calculation

For the magnetic field calculation the system of equations (1)-(3) for the magnetostatic problem has to be solved.

$$\nabla \times \boldsymbol{H} = \boldsymbol{J} \tag{1}$$

$$\nabla \cdot \boldsymbol{B} = 0 \tag{2}$$

$$\boldsymbol{B} = \mu_r \mu_0 \boldsymbol{H} + \mu_0 \boldsymbol{M} \tag{3}$$

where: $\boldsymbol{H}$ – magnetic field intensity, $\boldsymbol{J}$ – current density to due to movement of free charges, $\boldsymbol{B}$ – magnetic flux density, μ_0 – the permeability of free space and μ_r – relative permeability of the associated region.

Magnetic flux density can be represented with magnetic vector potential as in (4).

$$\boldsymbol{B} = \nabla \times \boldsymbol{A} \tag{4}$$

Calculation of Back Electromotive Force

Back electromotive force (EMF) of the AFPMSM at no-load is calculated using Faraday's law of electromagnetic induction based on the time variation of magnetic flux (5). The magnetic flux can be obtained through the magnetic flux density on the cross-section surface inside the coil which has to be perpendicular to the magnetic flux path (6).

$$e = -N \frac{\partial \phi}{\partial t} \tag{5}$$

$$\phi = \iint_S \boldsymbol{B} d\boldsymbol{S} \tag{6}$$

where: e – EMF, N – number of turns, $\partial\phi/\partial t$ – time variation of magnetic flux within the coil, S – surface.

Torque and force calculation

Forces are calculated using Maxwell's stress tensor method as in (7), (8) and (9).

$$\boldsymbol{F}_x = \iint_S \left(\frac{1}{\mu} \boldsymbol{B}_x \left(\boldsymbol{B} \cdot \boldsymbol{n} \right) - \frac{1}{2\mu} \left| \boldsymbol{B} \right|^2 \boldsymbol{n}_x \right) dS \tag{7}$$

$$\boldsymbol{F}_y = \iint_S \left(\frac{1}{\mu} \boldsymbol{B}_y \left(\boldsymbol{B} \cdot \boldsymbol{n} \right) - \frac{1}{2\mu} \left| \boldsymbol{B} \right|^2 \boldsymbol{n}_y \right) dS \tag{8}$$

$$\boldsymbol{F}_z = \iint_S \left(\frac{1}{\mu} \boldsymbol{B}_z \left(\boldsymbol{B} \cdot \boldsymbol{n} \right) - \frac{1}{2\mu} \left| \boldsymbol{B} \right|^2 \boldsymbol{n}_z \right) dS \tag{9}$$

where: n - normal to the surface.

Torque is calculated as a vector product of radius $\boldsymbol{r}$ and force $\boldsymbol{F}$ as in (10).

$$\boldsymbol{T} = \boldsymbol{r} \times \boldsymbol{F} \tag{10}$$

Torque around z-axis is calculated as in (11).

$$T_z = r_x F_y + r_y F_x \tag{11}$$

where: r_x – distance in x-axis, r_y – distance in y-axis.

Topologies of analysed AFPMSMs

Two topologies of the stator and the rotor of AFMPSMs are apart from the difference of stator windings completely the same. Even more, also the volume of cooper used for windings is the same in both cases. The detailed parameters of AFPMSMs are presented in Table 1.

Table 1. Parameters of AFPMSMs

		Single-layer AFPMSM	Double-layer AFPMSM
	Item	Value [unit]	Value [unit]
Stator	Number of coils	6	12
Stator	Number of turns	100	50
Stator	Wire diameter	1,23 [mm^2]	
Stator	Current	10 [A]	
Stator	Coil area width	20 [mm]	
Stator	Coil area height	15 [mm]	7,5 [mm]
Stator	Coil pitch	30 [deg]	
	Mechanical air-gap	1 [mm]	
Rotor	Disk radius	150 [mm]	
Rotor	Height of PMs	10 [mm]	
Rotor	Width of PMs	5 [mm]	
Rotor	Length of PMs	60[mm]	
Rotor	Number of poles	10	
Rotor	Number of rotor discs	2	
Rotor	Remanence of PMs	1,22 [T]	

To achieve a 10-pole machine, coils have to be connected in the way, which is presented for the single-layer windings presented in Fig. 2 and for the double-layer windings (Fig. 4). The number of poles is verified with a diagram of current density distribution in coil sides along the periphery of AFPMSM. Fig. 3 and 5 show a distribution of current density at the moment which corresponds to the time t=0.

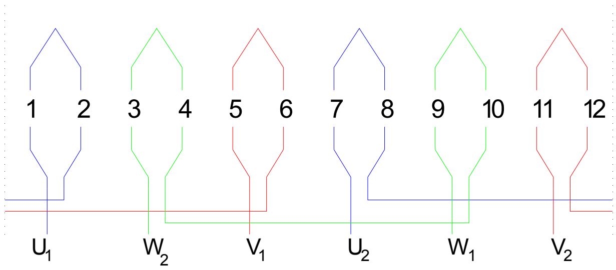

Fig.2. Connections between coils of single-layer stator windings

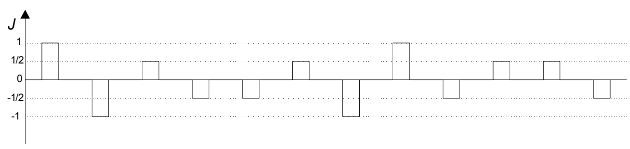

Fig.3. Distribution of current density in coil sides along the periphery of AFPMSM with single-layer stator windings at the moment which corresponds to t=0

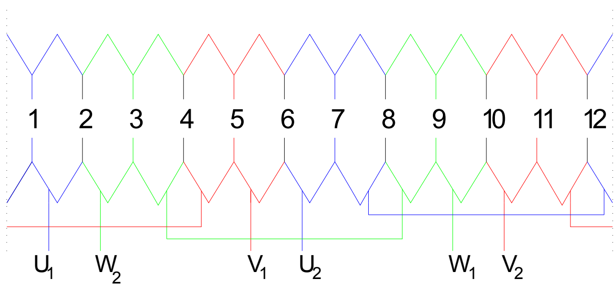

Fig.4. Connections between coils of double-layer stator windings

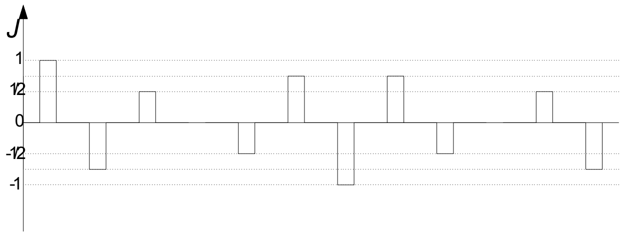

Fig.5. Distibution of current density in the coil sides along the periphery of AFPMSM with double-layer windings at the moment which corresponds to t=0

Figure 6 shows the star of slots, where $\underline{E}_1$, $\underline{E}_2$, $\underline{E}_3 \ldots \underline{E}_{12}$ are back EMFs phasors of the slots and α is electrical angle between two adjacent slots. Figure 7 shows the sum of connected sides of coils and the phase back EMFs. The sum of connected sides of coils is calculated on basis of connections presented in Fig. 2 and Fig. 4. The phase back EMFs are calculated for single-layer windings by using equations (12)-(14) and for double-layer windings with (15)-(17).

$$U=\left(E_1+E_2\right)\cdot\cos\left(\frac{\alpha}{2}\right)+\left(E_7+E_8\right)\cdot\cos\left(\frac{\alpha}{2}\right) \tag{12}$$

$$V=\left(E_5+E_6\right)\cdot\cos\left(\frac{\alpha}{2}\right)+\left(E_{11}+E_{12}\right)\cdot\cos\left(\frac{\alpha}{2}\right) \tag{13}$$

$$W=\left(E_9+E_{10}\right)\cdot\cos\left(\frac{\alpha}{2}\right)+\left(E_3+E_4\right)\cdot\cos\left(\frac{\alpha}{2}\right) \tag{14}$$

$$U=E_1+\frac{E_2}{2}\cdot\cos\alpha+\frac{E_{12}}{2}\cdot\cos\alpha+E_7+\frac{E_6}{2}\cdot\cos\alpha+\frac{E_8}{2}\cdot\cos\alpha \tag{15}$$

$$V=E_5+\frac{E_6}{2}\cdot\cos\alpha+\frac{E_4}{2}\cdot\cos\alpha+E_{11}+\frac{E_{12}}{2}\cdot\cos\alpha+\frac{E_{10}}{2}\cdot\cos\alpha \tag{16}$$

$$W=E_3+\frac{E_2}{2}\cdot\cos\alpha+\frac{E_4}{2}\cdot\cos\alpha+E_9+\frac{E_8}{2}\cdot\cos\alpha+\frac{E_{10}}{2}\cdot\cos\alpha \tag{17}$$

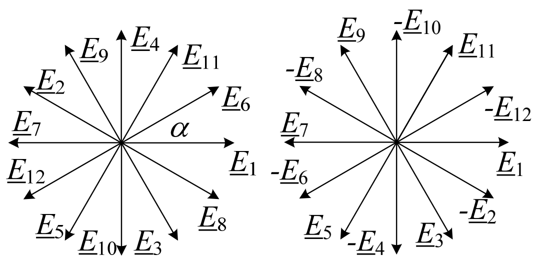

Fig.6. Star of slots

a)

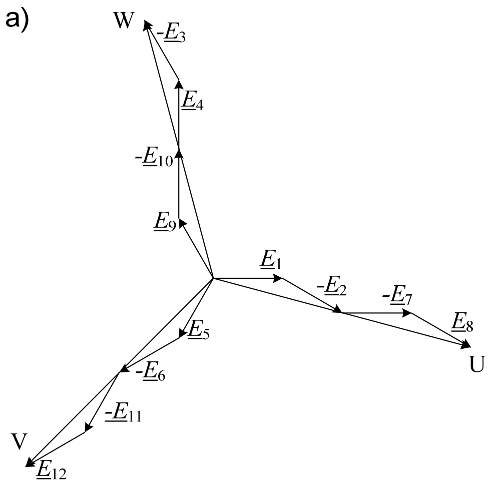

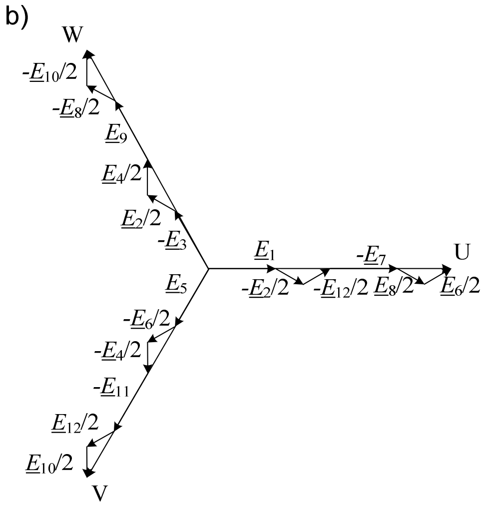

Fig.7. Vector sum of slots EMFs per phase for a) single-layer winding and b) double-layer winding (U, V and W are phase back EMFs)

Calculated results

Figures 8-17 show the results of calculations for AFPMSM with single-layer winding and with double-layer winding. The back electromotive force (back EMF) and the cogging torque were calculated at no-load and speed 1500 rpm. The detent force and the static torque were calculated at the load of 10 A, where the current density is 8.13 A/mm^2.

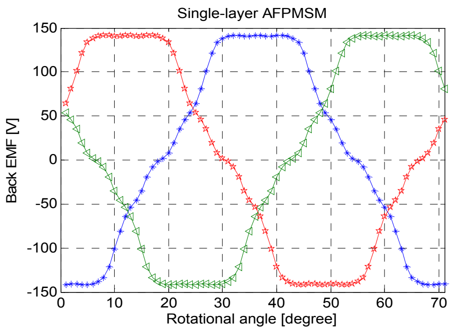

Fig.8. Back EMF of single-layer AFPMSM

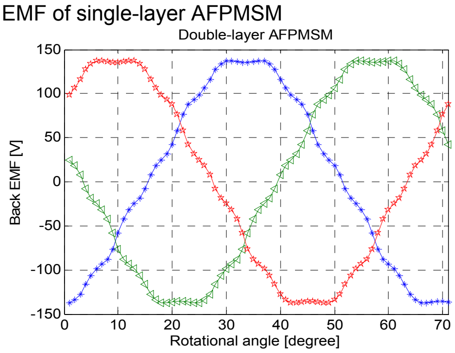

Fig.9. Back EMF of double-layer AFPMSM

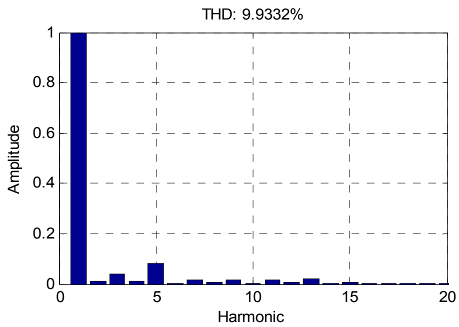

Fig.10. Back EMF harmonic components of single-layer AFPMSM

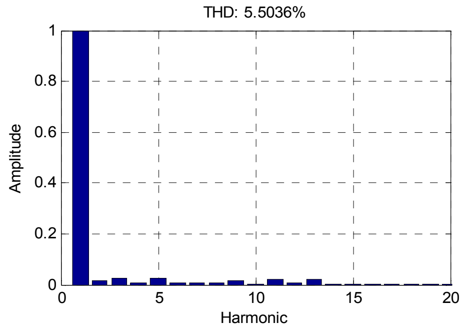

Fig.11. Back EMF harmonic components of double-layer AFPMSM

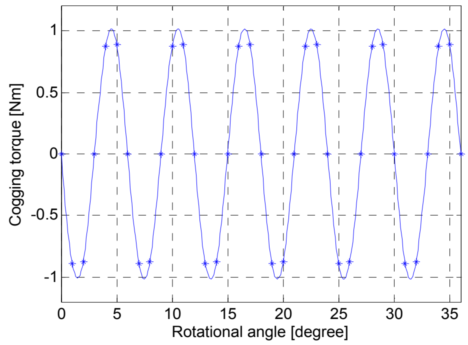

Fig.12. Cogging torque of single-layer AFPMSM

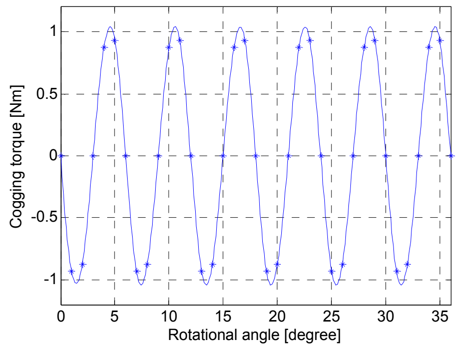

Fig.13. Cogging torque of double-layer AFPMSM

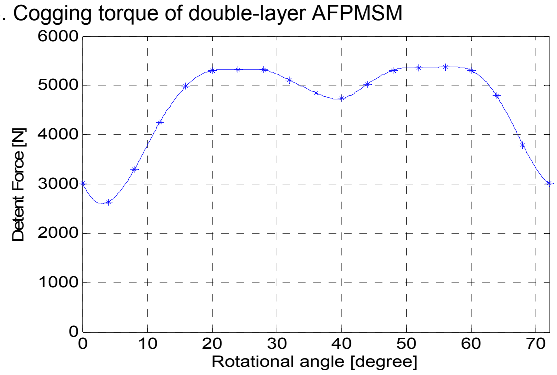

Fig.14. Detent force of single-layer AFPMSM

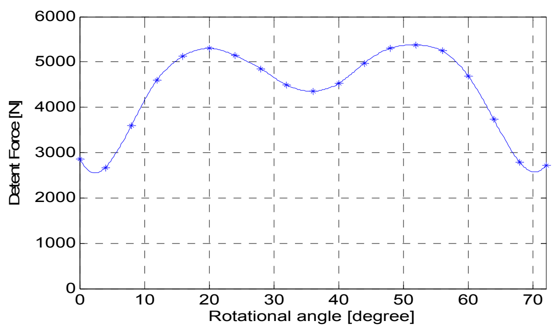

Fig.15. Detent force of double-layer AFPMSM

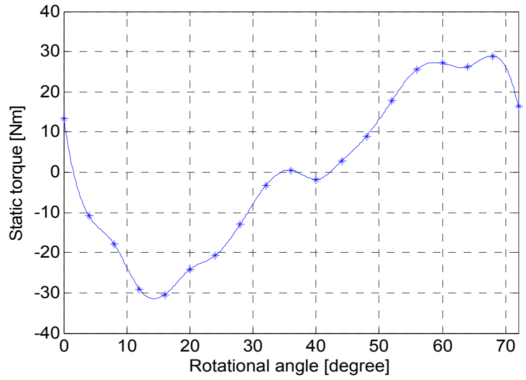

Fig.16. Static torque of single-layer AFPMSM

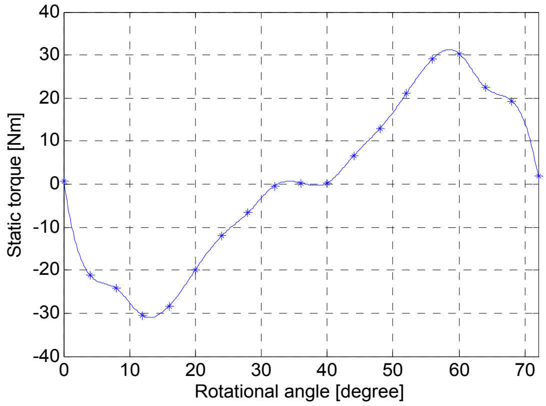

Fig.17. Static torque of double-layer AFPMSM

Conclusion

The comparison between calculated results of AFPMSMs with single- and double-layer windings shows that there is only a small difference in characteristics between these two machines. The main difference is in the shape and the peak value of back EMFs. The reason for that are the winding factors, which are a little bit smaller in case of double-layer windings and total harmonic distortion (THD), which is for 80% greater in case of single-layer windings. In addition to this investigation of the two types of windings a more detailed electromagnetic as well as thermal analysis can be done [12]. This more detailed investigation can be realised in order to have a complete picture about the performance abilities of the two types of windings.

REFERENCES

[1] Gieras J.F., Wang R.J., Kamper M.J., Axial flux permanent magnet brushless machines, *Springer* Science, second edition (2008).
[2] Zagirnyak M., Kalinov A., Romashykhina Zh., Diagnostic of broken rotor bars in induction motor on the basis of its magnetic field analysi, *Acta Technica Jaurinensis*, 6 (2013), No. 1, 115–125.
[3] Zagirnyak M., Mamchur D., Kalinov A., Comparison of induction motor diagnostic methods based on spectra analysis of current and instantaneous power signals, *Przeglad Elektrotechniczny*, 88 (2012), No. 12b, 221–224.
[4] Elez A., Car S., Maljković Z., A New Method for Inter-Coil Short Circuit Detection in Synchronous Machine Armature Winding, *International Review of Electrical Engineering-IREE*, 7 (2012) , No. 6; 6062-6069.
[5] Maljković Z.; Žarko D.; Stipetić S., Unsymmetrical load of a three-phase synchronous generator, *Przegląd Elektrotechniczny*, 89 (2013), No. 2b, 68-71.
[6] Zorman M., Pohorec S., Brumen B., Opening the knowledge tombs - web based text mining as approach for re-evaluation of machine learning rules, *Lecture notes in computer science*, 6295 (2010), 533-542.
[7] Brumen B., Jurič MB., Welzer-Družovec T., Rozman I., Jaakkola H., Papadopoulos A., Assessment of classification models with small amounts of data, *Informatica (Lith.)*, 18 (2007), No. 3, 343-362.
[8] Predin A., Biluš I., Hren G.. Possibilities for wind energy exploitation in Slovenia. *Journal of energy technology*, 4 (2011), No. 1, 39-48.
[9] Igrec D., Chowdhury A., Hadžiselimović M., Štumberger B., Measuring wind resources, *Journal of energy technology*, 4 (2011), No. 1, 49-59.
[10] Virtič P., Pišek P., Hadžiselimović M., Marčič T., Štumberger B., Torque analysis of an AFPMSM by using analytical magnetic field calculation, *IEEE Transactions on Magnetics*, 45 (2009), No. 3, 1036-1039.
[11] Virtič P., Pišek P., Marčič T., Hadžiselimović M., Štumberger B., Analytical analysis of magnetic field and back electromotive force calculation of an axial-flux permanent magnet synchronous generator with coreless stator, *IEEE Transactions on Magnetics*, 44 (2008), No. 11, 4333-4336.
[12] Cvetkovski G., Petkovska L., Gair S., Combined Electromagnetic and Thermal Analysis of Permanent Magnet Disc Motor, Studies on Computational Inteligence, *Intelligent Computer Techniques in Applied Electromagnetics, Springer*, 119 (2008), 259-268.

***Authors**: assist. Jan Šlamberger B. Sc. E. E., University of Maribor, Faculty of Energy Technology, Hočevarjev trg 1, 8270 Krško, Slovenia, E-mail: jan.slamberger@uni-mb.si; assoc. prof. Mario Vražić, Ph.D., University of Zagreb, Faculty of electrical engineering and computing, Unska 3, 10000 Zagreb, Croatia, E-mail: mario.vrazic@fer.hr; assoc. prof. Peter Virtič, Ph.D., University of Maribor, Faculty of Energy Technology, Hočevarjev trg 1, 8270 Krško, Slovenia, E-mail: peter.virtic@uni-mb.si.*